Article

Determination of Accuracy and Usability of a SLAM Scanner GeoSLAM Zeb Horizon: A Bridge Structure Case Study

Rudolf Urban [1,*], Martin Štroner [1], Jaroslav Braun [1], Tomáš Suk [1], Ľudovít Kovanič [2] and Peter Blistan [2]

[1] Department of Special Geodesy, Faculty of Civil Engineering, Czech Technical University in Prague, Thákurova 7, 16629 Prague, Czech Republic; martin.stroner@fsv.cvut.cz (M.Š.); jaroslav.braun@fsv.cvut.cz (J.B.); tomas.suk@fsv.cvut.cz (T.S.)

[2] Institute of Geodesy, Cartography and Geographical Information Systems, Faculty of Mining, Ecology, Process Control and Geotechnologies, Technical University Kosice, Park Komenského 19, 04001 Košice, Slovakia; ludovit.kovanic@tuke.sk (Ľ.K.); peter.blistan@tuke.sk (P.B.)

* Correspondence: rudolf.urban@fsv.cvut.cz

Abstract: The presented paper focuses on testing the performance of a SLAM scanner Zeb Horizon by GeoSLAM for the creation of a digital model of a bridge construction. A cloud acquired using a static scanner Leica ScanStation P40 served as a reference. Clouds from both scanners were registered into the same coordinate system using a Trimble S9 HP total station. SLAM scanner acquisition was performed independently in two passes. The data acquired using the SLAM scanner suffered from relatively high noise. Denoising using the MLS (Moving Least Squares) method was performed to reduce noise. An overall comparison of the point clouds was performed on both the original and MLS-smoothed data. In addition, the ICP (Iterative Closest Point) algorithm was also used to evaluate local accuracy. The RMSDs of MLS-denoised data were approximately 0.02 m for both GeoSLAM passes. Subsequently, a more detailed analysis was performed, calculating RMSDs for several profiles of the construction. This analysis revealed that the deviations of SLAM data from the reference data did not exceed 0.03 m in any direction (longitudinal, transverse, elevation) which is, considering the length of the bridge of 133 m, a very good result. These results demonstrate a high applicability of the tested scanner for many applications, such as the creation of digital twins.

Keywords: GeoSLAM; accuracy; bridge

1. Introduction

The creation of digital models (or digital twins [1]) has become a hot topic, especially since the advent of BIM (Building Information Management) [2]. An accurate and complete digital model of a building is the cornerstone of data management of all BIM participants in the construction process [3,4], necessitating the use of geodetic methods. These methods provide sufficient accuracy for producing digital models in the mandatory regional coordinate system legislatively prescribed for data management.

Laser scanning [5] and photogrammetry [6] undoubtedly count among the main geodetic methods for creating a digital model. Both these mass data collection methods can be static or mobile, depending on whether the sensor is mounted on a mobile platform (ground vehicle, airborne carrier) or not.

Ground-based data acquisition (static) usually excels in high accuracy and complexity (completeness) of the resulting model, as reported, e.g., by [7,8]. Aerial data acquisition, in turn, is highly suitable for large objects or areas [9–11], where fast acquisition is necessary, but is not suitable for interiors or parts of the objects that are obstructed in the aerial view (such as pillars of a bridge structure) due to the lack of a GNSS location signal; however, this obstacle can also be overcome as shown, e.g., in [12–14]. Mobile data collection partly combines the speed of aerial data collection with the complexity of ground-based data collection [15,16] at the cost of slightly worse accuracy, as shown in [17,18].

Photogrammetric methods have also become very popular lately. These methods depend mainly on the sensor and good illumination of the object. As a rule, they benefit from relatively low acquisition costs of the sensor itself, but quite a few prerequisites must be met to produce a usable point cloud, such as suitable sensing methodology [19], the choice of ground control points (GCPs) [20], the selection of the sensor (based on the required ground sampling distance) [21], etc. The used software can undoubtedly also influence the quality of the resulting model [22].

In some cases, however, even seemingly correctly performed measurements fail to yield satisfactory results—for example, the model may be distorted, or the image correlation may be unsuccessful. Consequently, it is always advisable to perform a verification of the model using classical geodetic methods or another bulk data collection method [23].

Compared to photogrammetry, laser scanning is generally associated with higher acquisition costs of the equipment, but if the technology is used correctly, the resulting digital model is usually correct in shape [24]. Point clouds are registered (combined) using control points or direct cloud-to-cloud algorithms (such as the iterative closest point, ICP, algorithm) [25,26]. This technology can be used at night; if this is the case, however, the colors of the points are incorrectly presented, unless additional illumination is used.

Bridge structures are often complicated objects for data collection [27] as they can be relatively long and tall, contain both horizontal and vertical elements, and often are curved in shape [28]. Importantly, considering extremely high requirements on the life span of bridges, the accuracy requirements on geodetic measurements of such objects are typically very high [29].

The progress in the field of laser scanning brought about the development of SLAM (Simultaneous Localization and Mapping) scanners, the use of which can be potentially advantageous for some types of bridge structures. This technology works by using laser rangefinders, usually mounted on a rotating head, and an IMU (inertial measurement unit). The combination of data acquired from both sensors is then used to create a point cloud characterizing the environment while determining the trajectory of the entire system based on the knowledge of its previous position and newly acquired sensor data. In this way, the system trajectory is mapped incrementally, which, however, necessarily leads to a loss of accuracy with increasing distance [30]. The resulting accuracy of the model is, therefore, determined not only by the accuracy of the sensors themselves but also by the quality of the algorithm calculating the trajectory [31]. One important advantage of this system when comparing it to static scanners lies in the fact that the gradual movement while scanning enables the elimination of shadowing/obstruction, which is particularly beneficial for complex or rugged objects [32].

This paper aims to test the performance of the SLAM technology in creating a digital model of a bridge. In view of the complexity of the used bridge structure, the emphasis will be put on the accuracy of the acquired cloud (especially in terms of the spatial relationships of the individual parts of the bridge) along with the assessment of the local quality of the cloud (especially noise). The accuracies of the positions of the piers and of horizontal parts of the bridge will be also compared. Furthermore, the characteristics of the acquired data (noise) will be investigated, and the use of a smoothing (denoising) procedure for improving the digital model quality will be proposed and tested.

2. Materials and Methods

A SLAM scanner Zeb Horizon GeoSLAM (Orlando, FL, USA) was used for the acquisition of data on a bridge structure, and the results were compared with a reference cloud obtained using a Leica ScanStation P40 (Heerbrugg, Switzerland) terrestrial laser scanner to be able to point clouds in the selected profiles. The pillars could then be compared to each other.

To enable the comparison of the selected profiles of both clouds and the pillars, both clouds were georeferenced to the same coordinate system using ground control points (GCPs). The GCP positions were determined using a Trimble S9 HP (Westminster, CO,

USA) total station. Finally, a processing procedure for the raw SLAM data was proposed, the aim of which was to significantly improve (de-noise) the data.

2.1. Testing Area

The testing was performed in the Czech Republic, on a bridge construction on the bypass of the Církvice village (road No. I/38; Figure 1). This new reinforced concrete bridge with four spans is, in total, 133 m long, and its height above the terrain is approximately 7 m. As the surface of the bridge was undergoing final operations prior to being open for use, only the lower structure of the bridge was used for testing of the Zeb Horizon GeoSLAM scanner.

Figure 1. The testing bridge and its location.

2.2. Used Instruments

Laser scanning of the bridge structure was performed with a Zeb Horizon scanner by GeoSLAM (Figure 2a). This scanner uses the SLAM technology and, according to the manufacturer, achieves a relative accuracy of 0.01–0.03 m. The scanning speed is 300,000 points/second with a range of up to 100 m.

(a) (b)

Figure 2. (**a**) Mobile laser scanner Zeb Horizon by GeoSLAM and (**b**) static laser scanner ScanStation P40 by Leica.

Reference data for evaluation of the accuracy were obtained by terrestrial scanning with a Leica ScanStation P40, a terrestrial scanner (Figure 2b) with a field of view of

$360° \times 270°$, distance measurement accuracy of 1.2 mm + 10 ppm, angle accuracy of $8''$, liquid compensator with an accuracy of $1.5''$, maximum measurement range of 270 m (considering 18% reflectance), and scanning speed of 1 million points per second.

High accuracy georeferencing of ground control points was performed with a Trimble S9 HP total station, characterized by standard deviations of 0.3 mgon of angle measurement and 0.8 mm + 1 ppm in length, respectively.

A Trimble R2 GNSS RTK (Westminster, CO, USA) receiver (dual-frequency, receives GPS, Glonass, Galileo, and BeiDou satellite system signals; for the RTK network, the horizontal accuracy is expressed as RMSE of 10 mm + 0.5 ppm, vertical accuracy of 20 mm + 0.5 ppm, respectively) with a Trimble TSC3 controller (Westminster, CO, USA) were used for the total station reference measurements.

2.3. Terrestrial Measurements and Data Acquisition

The terrestrial measurements were linked to the reference systems of the Czech Republic (S—JTSK, Bpv) using three temporary points determined by a GNSS RTK Trimble R2 receiver with corrections from the CZEPOS virtual reference station system. These temporary points were subsequently georeferenced using the Trimble S9 HP total station, which was employed to determine ground control points for the laser scanners. In this way, an identical coordinate system was ensured for point clouds from both scanners, facilitating their comparison.

The lower structure of the bridge was scanned with a Leica ScanStation P40 from 15 scanning positions at a density of 6 mm/10 m using a total of 7 GCPs (Leica GZT21 black and white 4.5-inch diameter targets; Figure 3, points 1–7) georeferenced using a Trimble S9 HP total station. In addition, 10 highly reflective 0.5×0.5 m targets (Figure 4, points 1001–1010) were georeferenced in the same way to enable the transformation of the clouds from the Zeb Horizon scanner into the required coordinate system. All measurements were made from two positions of the total station.

Figure 3. Overview of the (ground) control points. Here, 1–7 indicate vertical black and white targets serving as ground control points (GCPs) for the Leica P40 scanner (red), and 1001–1010 are horizontal targets used as GCPs for SLAM cloud transformation into the Czech coordinate systems (white).


Figure 4. The reference cloud obtained using Leica ScanStation P40 colored according to the intensity of the reflected signal.

The point cloud obtained by the Leica ScanStation P40 laser scanner was considered as the reference cloud (Figure 4).

Two point clouds of the lower bridge structure (GeoSLAM 1 and GeoSLAM 2) were acquired using the Zeb Horizon scanner (the data from GeoSLAM 1 are shown in Figure 5)

using the same trail (each cloud was created during a separate round trip) leading approximately 10 m from the construction. The collection of photographic data was turned off during data acquisition. To further improve the accuracy, ten stops were performed during each pass on so-called alignment points in accordance with the manufacturer's instructions.
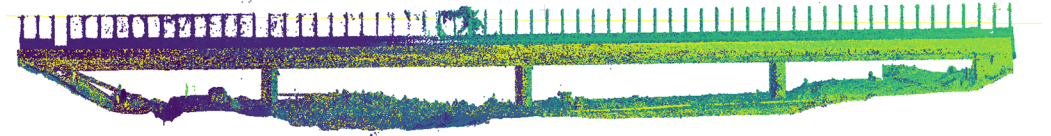

Figure 5. The cloud obtained using the GeoSLAM Zeb Horizon scanner colored according to the intensity of the reflected signal.

2.4. Data Processing

First, the position of the total station was computed using the free position method and auxiliary points determined by the Trimble R2 GNSS receiver. All coordinates of other points (GCPs, control points) were calculated using the polar method. The data acquired with Leica P40 were processed in the Leica Cyclone software ver. 2023.0.1. The individual scans were automatically georeferenced to the black-and-white GCPs. The average registration error was 1.8 mm.

The Zeb Horizon data were first processed in the local coordinate system in the manufacturer-provided software GeoSLAM Connect ver. 2.3.0. To be able to compare the cloud with the reference one, it was transformed into the Czech coordinate system using square high-reflection targets with georeferenced centers serving as GCPs. These targets were used, for example, in [33], where the transformation method is described in detail. Figure 6 shows the scanned target and its color coding based on the intensity. In principle, the points representing the targets were filtered from the cloud, their centers were determined as the centers of gravity, and these coordinates (georeferenced previously with the total station) were used for spatial transformation (translation in x,y,z-axes, rotation about the same axes). Out of the ten horizontal targets (1001–1010), seven that were sufficiently captured by the SLAM scanner were used for the transformation.
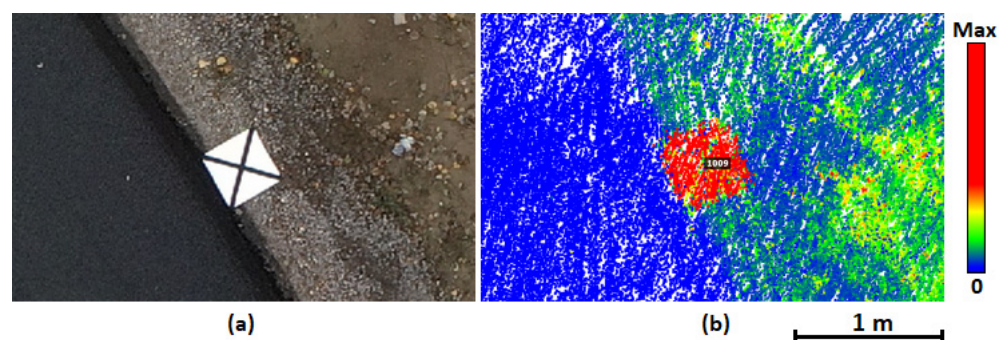

Figure 6. An example of the targets used as GCPs for the transformation of the GeoSLAM point cloud into the Czech georeferencing system. (**a**) Black and white scan; (**b**) the target color-coded according to the reflection intensities.

2.5. Precision and Accuracy Evaluation

To evaluate the accuracy of the Leica P40 reference cloud, we created an additional 21 control points (CPs) georeferenced using the total station (see Figure 7 for the placement of these CPs). The accuracy was expressed as the root mean square deviation (*RMSD*) between these points and the closest surface of a triangular network created from the nearest 15 points from the Leica P40 point cloud:

$$RMSD = \sqrt{\frac{\sum_1^n d_i^2}{n}} \tag{1}$$

where d is the minimum distance between the tested point (be it a control point or a point from a cloud) and the surface of a local TIN network created from the reference cloud (Leica P40), and n is the number of points in the tested cloud.
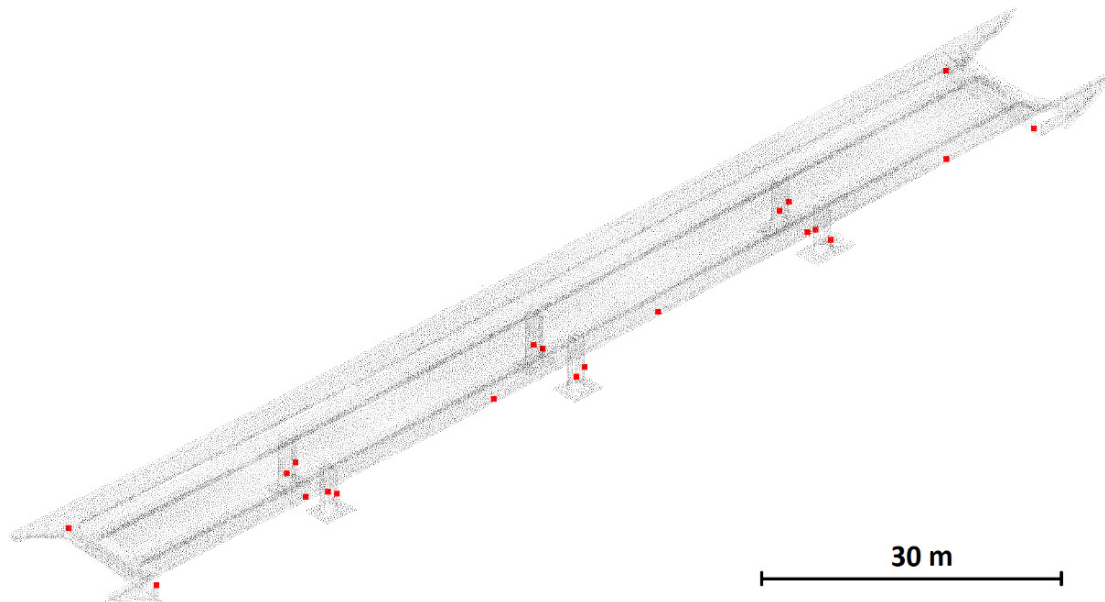
Figure 7. Locations of control points on the bridge (red dots).

Further, the accuracy of the transformation of both GeoSLAM clouds into the Czech coordinate system using high-reflection targets for further comparisons was evaluated using root mean square error (*RMSE*), defined as:

$$RMSE = \sqrt{\frac{\sum_{i=1}^n \left(e_{x_i}^2 + e_{y_i}^2 + e_{z_i}^2\right)}{3n}} \tag{2}$$

where e_x, e_y, and e_z are coordinate corrections of GCPs in the GeoSLAM cloud after its transformation into the Czech coordinate system from the same points georeferenced using the total station, and n is the number of points.

For further processing, the data were cropped and cleaned to capture solely the bridge structure. Leica P40 (reference) data were cropped to capture a slightly larger area to prevent any issues with evaluation on the edges of the cloud. If any part of the bridge was not captured in the reference data (e.g., due to obstruction by vegetation), it was also removed from the GeoSLAM data.

Further evaluation was performed in two main stages:

1. Evaluation of the overall agreement by comparing the Zeb Horizon cloud with the reference cloud from the Leica P40

    a. Absolute comparison (includes the effect of inaccuracy in the determination of GCPs)
    b. Relative comparison (comparison of shape and size—after ICP transformation of the whole GeoSLAM cloud on the reference cloud)

2. Local profile-by-profile evaluation for determining local deformations

    a. Absolute (overall profile location, showing local systematic errors)
   b. Relative (determination of local deformation and local accuracy)

RMSD (Equation (1)) was used as the accuracy parameter for all cloud comparisons.

In view of the fact that Zeb Horizon clouds suffer from relatively high noise (with a maximum variance of 10–12 cm on a planar surface), it seems pertinent to smooth the data out. The Moving Least Squares (MLS) smoothing method seems to be a suitable way for such denoising [34] before further use. For this reason, the whole comparison was performed twice—separately for the original data and for data smoothed using this method.

The clouds were processed and compared in the freely available software CloudCompare ver. 2.12.4. The Compute cloud/cloud distance function based on creating a local triangular network from the 15 nearest points (Local modeling tab, Local model option— 2D1/2 Triangulation) was used for cloud comparison. The "Smooth using MLS function" (in the Plugins/PCL wrapper menu, according to [34]) command with the neighborhood size (search radius) set to 0.15 m, Polynomial Order 2 and Squared Gaussian Parameter 0.0009 (corresponding to a standard length measurement of 0.03 m) were used for smoothing. The clouds produced in this way were called GeoSLAM 1-MLS and GeoSLAM 2-MLS, respectively.

The Fine Registration ICP function (Tools/Registration menu) was used for the ICP transformation of the clouds. The *RMSD* difference parameter determining the difference of termination of the iterative computation was set to 5×10^{-7}, with 1 million points used as a sample for this evaluation (random sampling limit). The evaluation of individual profiles was performed using all points in the individual profile. Due to the likely presence of outlying points, the "enable farthest point removal" option was activated. The ICP comparison served to evaluate the shape of the cloud without being burdened by a possible georeferencing error.

In addition, we used nine evaluation profiles where ICP transformation was performed only locally for the individual profiles to remove a potential global distortion of the cloud and evaluate the local accuracy. The evaluation profiles are depicted in Figure 8 (red). They were selected to cover all pillars and half the distance between them. The width of all profiles was 5 m, the only exceptions being the profiles of the initial and terminal supports, which were about half that width.
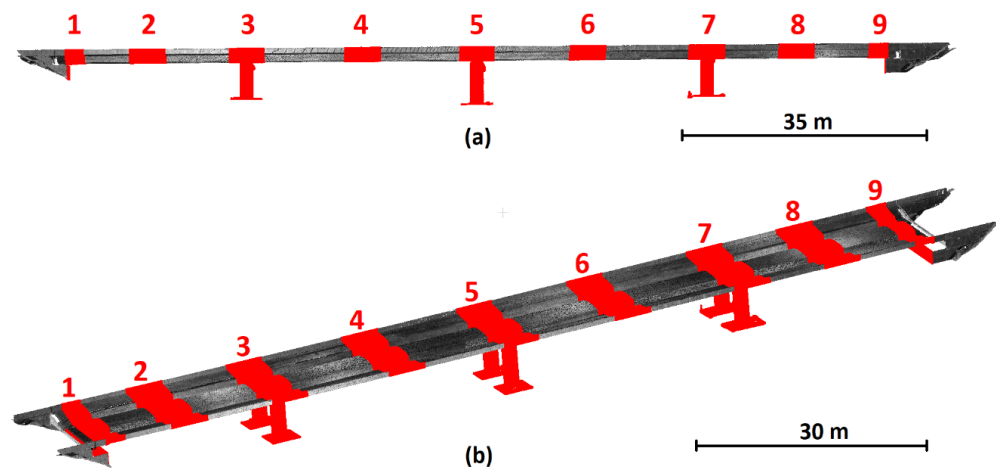
Figure 8. Profiles marked with numbers for local evaluation highlighted in the cloud; (**a**) side view and (**b**) oblique view.

A flowchart summarizing the data measurement and processing procedure is given in Figure 9.
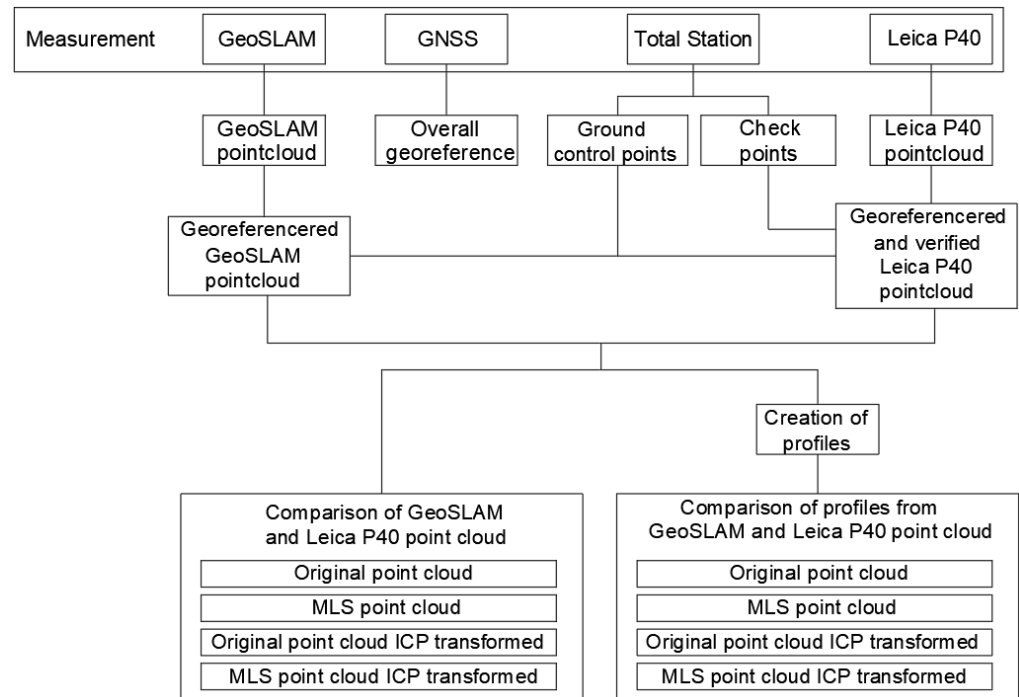
Figure 9. Flowchart summarizing the data measurement and processing procedure.

3. Results

The verification of the accuracy of the reference cloud (Leica P40) using 21 control points independently georeferenced using the Trimble S9 HP total station proved high accuracy of that cloud, with an *RMSD* of 0.005 m. In view of the manufacturer-declared SLAM scanner accuracy (0.01–0.03 m), the reference cloud accuracy was sufficient.

The reference point cloud was also diluted to a resolution of 3 mm (the distance of neighboring points of 3 mm or less) using the Subsample, a point cloud function in Cloud Compare. The diluted cloud contained 39,078,802 points. The GeoSLAM 1 and GeoSLAM 2 clouds were not diluted, containing 19,605,824 and 8,170,880 points, respectively. The number of GCPs for calculations of the transformation parameters is shown in Table 1.

Table 1. Characteristics of point clouds and results of point cloud transformation to the Czech coordinate system.

Data	Number of Points	Subsampling [m]	Number of GCPs	RMSE [m]	Acquisition Time	Processing Time
Leica P40	39,078,802	0.003	7	0.003	3 h	30 min
GeoSLAM 1	19,605,824	-	7	0.059	30 min	45 min
GeoSLAM 2	8,170,880	-	7	0.064	30 min	45 min

Figure 10 shows a cross-section of one of the pillars, enabling a visual comparison of the Leica P40 reference cloud, GeoSLAM 1 cloud, and the denoised GeoSLAM 1-MLS cloud. The differences in quality are obvious, especially for the un-smoothened GeoSLAM cloud suffering from substantially greater noise, the magnitude of which, moreover, differed throughout the object (which was probably associated with the distance between the scanner and the object at the moment of scanning of the respective part). GeoSLAM MLS data were much smoother; however, rounding of corners could be noted (resulting both from the uncertainty in the input data and from the surface approximation).
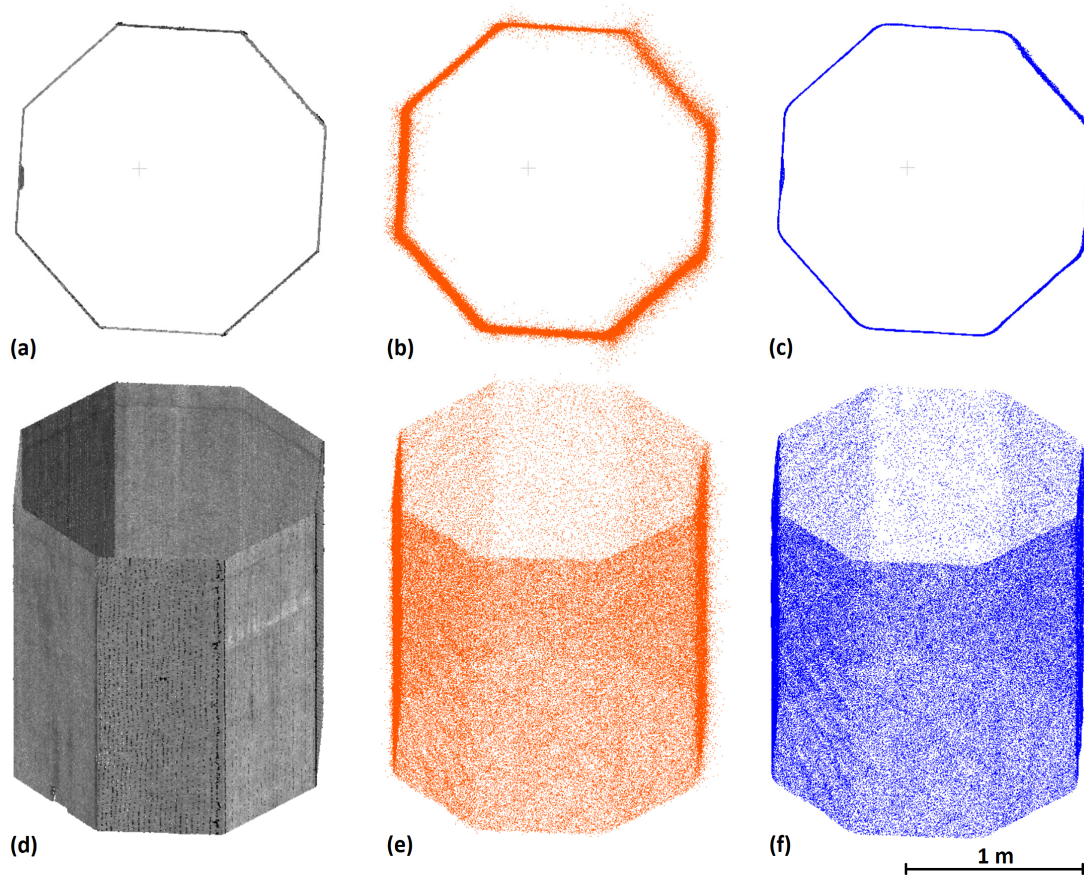
Figure 10. Visualization of the pillar point cloud—top view—acquired by (**a**) P40, (**b**) GeoSLAM, and (**c**) GeoSLAM-MLS, and the same in izometric view: (**d**) P40, (**e**) GeoSLAM, and (**f**) GeoSLAM-MLS.

Next, we evaluated the overall agreement between the GeoSLAM and reference clouds. The results (*RMSDs*) are shown in Table 2. These global characteristics showed a very good agreement of the GeoSLAM clouds with the reference cloud. Denoising by MLS improved the accuracy in all comparisons, although not to a major degree, which was understandable in view of the magnitude of the noise (see also Figures 11 and 12).

Table 2. Comparison of whole GeoSLAM and P40 clouds.

| Data	Original Cloud RMSD [m]	Denoised (MLS) Cloud RMSD [m]	Original Data ICP RMSD [m]	Denoised (MLS) Data ICP RMSD [m]
GeoSLAM 1	0.021	0.017	0.015	0.010
GeoSLAM 2	0.025	0.023	0.019	0.015

In general, the high noise of GeoSLAM Zeb Horizon clouds "hides" the possible systematic differences (Figure 10). MLS-smoothed data were much clearer. For this reason, only MLS-smoothed data will be discussed further as they could better reveal the systematic distortions of the clouds.

Figures 11 and 12 visualize the comparison to the reference cloud of MLS data and for MLS/ICP data. Both passes with the GeoSLAM Zeb Horizon scanner showed the same pattern, with better accuracies at the beginning and end of the bridge, while in the middle of the bridge, the accuracy was lower and *RMSDs* reached up to 0.04 m. For ICP-transformed clouds (bottom panels of Figures 11 and 12), the *RMSDs* were generally lower, but the shape (and/or size) of the GeoSLAM cloud differed from that of the reference one. *RMSDs* were bigger at the beginning and end of the bridge (up to 0.05) and smaller in the middle

(0.02 and better). This comparison, however, only shows the global characteristics (the distance between clouds) and contains no information on the direction of the deviation. For this reason, we also performed a profile-by-profile comparison after a local ICP transformation. The results of this comparison are presented in Tables 3 and 4 and visualized in Figures 13 and 14.
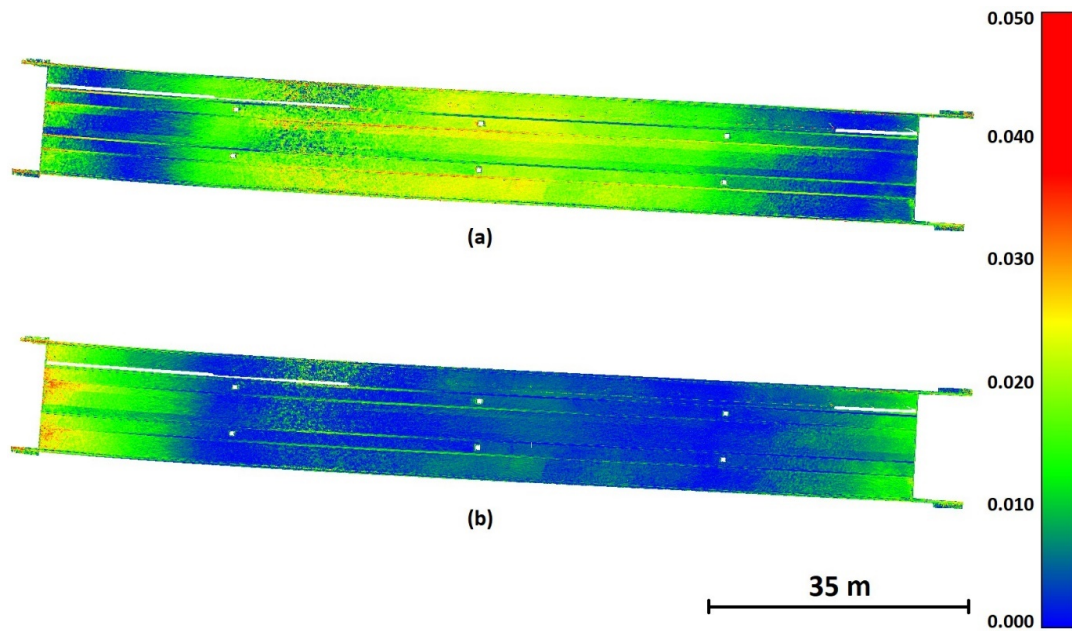
Figure 11. Distances of GeoSLAM 1-MLS data from the P40 reference cloud: (**a**) the SLAM cloud transformed solely based on GCPs; (**b**) SLAM cloud transformed using the ICP transformation.
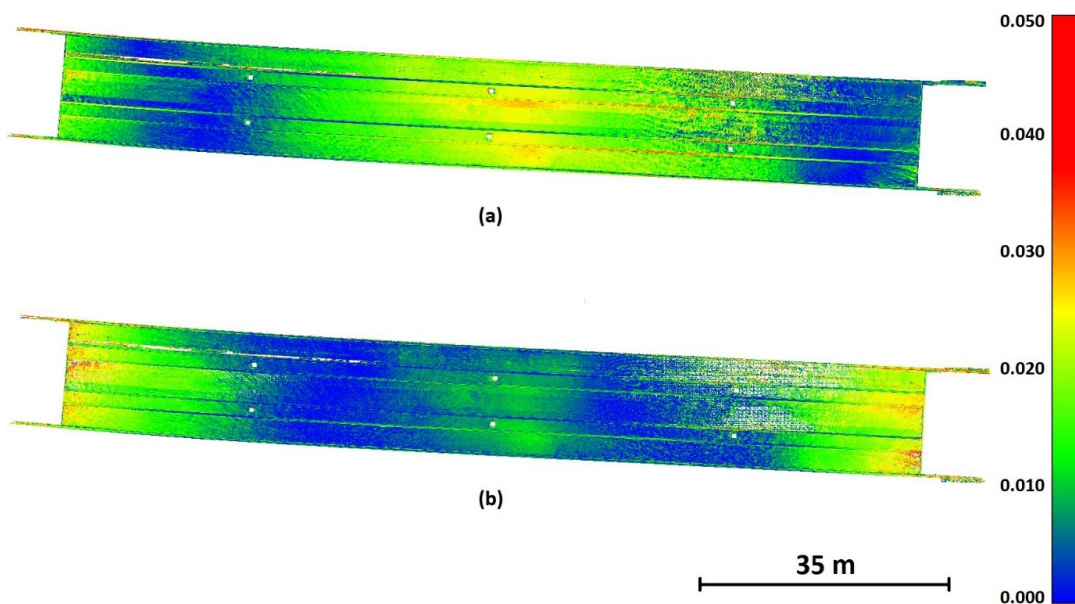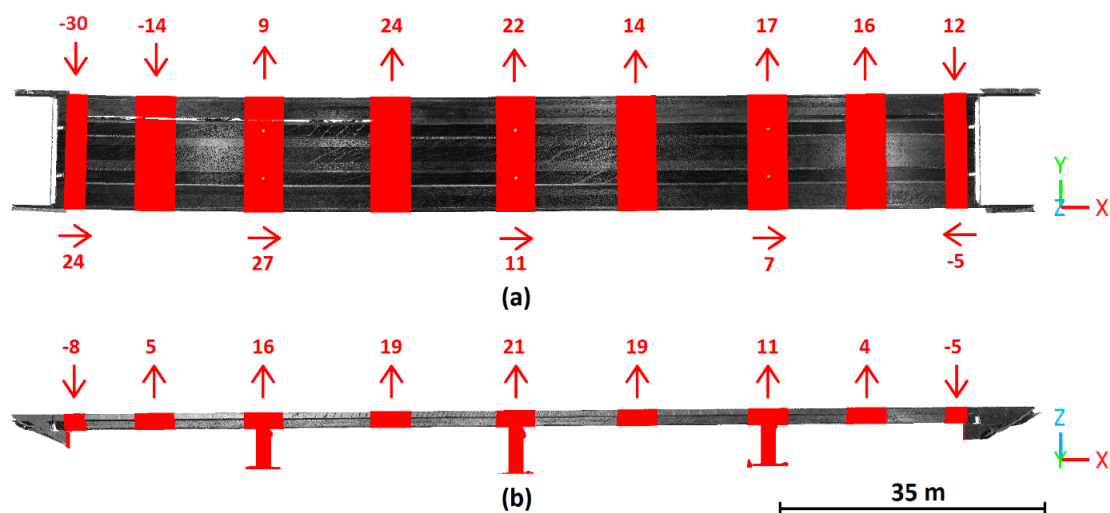

Figure 12. Distances of GeoSLAM-2 MLS data from the P40 reference cloud: (**a**) the SLAM cloud transformed solely based on GCPs; (**b**) SLAM cloud transformed using the ICP transformation.

Table 3. Results of the evaluation of individual profiles in GeoSLAM 1 data compared to the Leica P40 reference cloud in individual directions (in meters).

Data	GCP-Transformed					ICP-Transformed	
	Original RMSD	MLS RMSD	Shift dX_{MLS}	Shift dY_{MLS}	Shift dZ_{MLS}	Original RMSD	MLS ICP RMSD
1	0.028	0.024	0.024	−0.030	−0.008	0.015	0.005
2	0.013	0.010		−0.014	0.005	0.009	0.005
3	0.023	0.018	0.027	0.009	0.016	0.014	0.006
4	0.030	0.023		0.024	0.019	0.019	0.006
5	0.023	0.020	0.011	0.022	0.021	0.011	0.005
6	0.022	0.019		0.014	0.019	0.012	0.004
7	0.020	0.014	0.007	0.017	0.011	0.015	0.005
8	0.016	0.010		0.016	0.004	0.013	0.004
9	0.014	0.008	−0.005	0.012	−0.005	0.011	0.004
Mean	0.020	0.014	-	-	-	0.013	0.005

Table 4. Results of the evaluation of individual profiles in GeoSLAM 2 data compared to the Leica P40 reference cloud in individual directions (RMSDs in meters).

Data	GCP-Transformed					ICP-Transformed	
	Original RMSD	MLS RMSD	Shift dX_{MLS}	Shift dY_{MLS}	Shift dZ_{MLS}	Original RMSD	MLS ICP RMSD
1	0.021	0.018	0.006	−0.033	−0.017	0.013	0.005
2	0.016	0.014		−0.021	−0.004	0.010	0.006
3	0.017	0.011	0.009	−0.002	0.010	0.015	0.006
4	0.024	0.021		0.011	0.022	0.012	0.005
5	0.028	0.026	−0.007	0.025	0.031	0.012	0.005
6	0.031	0.027		0.027	0.026	0.013	0.005
7	0.038	0.028	−0.015	0.035	0.019	0.024	0.010
8	0.018	0.013		0.023	0.002	0.009	0.005
9	0.017	0.014	−0.013	0.005	−0.007	0.010	0.005
Mean	0.022	0.017	-	-	-	0.012	0.005

Figure 13. Shifts of GeoSLAM 1−MLS data from the reference cloud in millimeters (Table 4): (**a**) shifts dX_{MLS} and dY_{MLS}, (**b**) shift dZ_{MLS}.
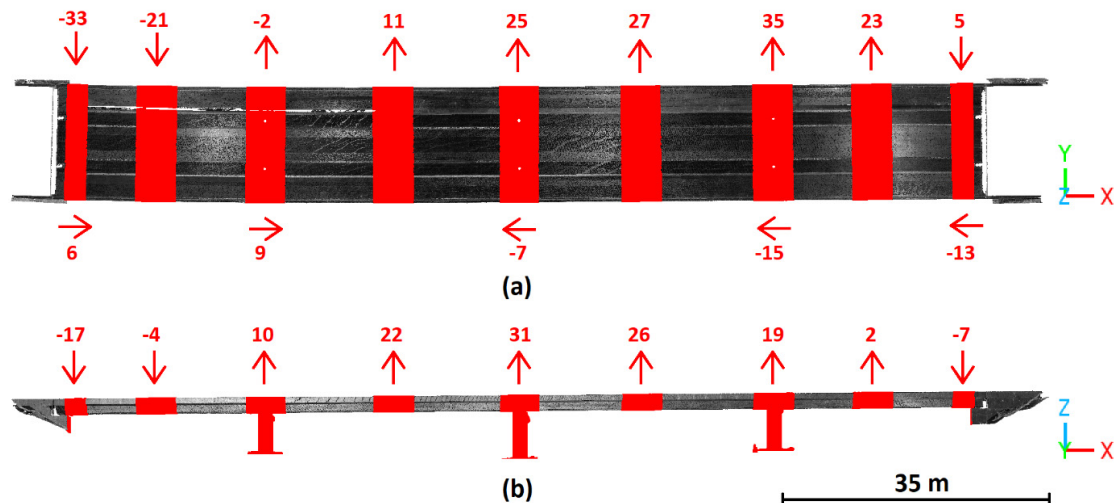
Figure 14. Shifts of GeoSLAM 2−MLS data from the reference cloud in mm (Table 4), (**a**) shifts dX_{MLS} and dY_{MLS}, (**b**) shift dZ_{MLS}.

Tables 3 and 4 show the gradual changes in the errors of the GeoSLAM clouds compared to the reference. The deviations were calculated for individual profiles (bridge pillars, supports, and central parts of the bridge between the pillars). For pillars and supports, shifts were calculated in all three axes (longitudinal shift dX, transverse shift dY, and elevation shift dZ), while in the profiles not directly supported by pillars, only the transverse error dY and elevation error dZ were calculated. The results are visualized in Figures 13 and 14. We can see that in both passes, the maximum deviation from the reference cloud in any individual direction was 0.035 m. Mean errors for both clouds were below 0.015 m and, when applying ICP, as little as below 0.01 m.

4. Discussion

We surveyed a bridge structure using a high-accuracy static scanner and used the thus acquired cloud to evaluate those produced by a SLAM scanner Zeb Horizon by GeoSLAM to determine the accuracy that can be achieved by this type of scanner. The bridge structure was selected for the survey because of its complex shape with numerous projections and irregular shapes. To assess the effect of data processing on the results, we also used MLS data smoothing. In addition, to remove the influence of possible georeferencing errors, we also used the ICP algorithm to better illustrate the local accuracy of the data.

The SLAM scanner data were characterized by much greater noise than the static scanner cloud. On the other hand, SLAM scanners can achieve better area coverage as the scanner location keeps moving, which eliminates obstructions.

The shape accuracy of the resulting cloud remains a crucial parameter of the acquired cloud. Importantly, it often depends on the correct function of the algorithm in the respective environment. Many studies have investigated the accuracy of the SLAM technology; unfortunately, few are truly conclusive.

Testing of SLAM technology has been addressed, for example, in [31], where the quality of point clouds acquired by different SLAM algorithms was evaluated. The achieved accuracies of the results were several centimeters to decimeters; however, these accuracies were simply obtained by comparing distances measured in the field to distances measured in the cloud. Given the laborious nature of field distance measurements, this approach led to a number of distances insufficient for a reliable statistical evaluation.

Similarly, Tiozzo Fasiolo et al. [35] compared the results of mapping using SLAM scanners mounted on robotic rovers, employing also different algorithms, with the results obtained by a terrestrial scanning system. They reported an average accuracy of 0.05 m *RMSE*; however, in the case of a long narrow corridor, the deviations were around 0.1 m.

Wajs et al. [36] tested the GeoSLAM scanner for mapping subterranean spaces and reported *RMSDs* of 5–6 cm; however, their comparison was just between two measurements with the same scanner, not with more accurate reference data. As our comparison of two passes with the scanner (see Tables 3 and 4) demonstrated, such a design is unfortunate as both passes may suffer from identical systematic errors and thus yield a good agreement between the passes even though the deviations from the reality (in our case, the reference cloud) are higher.

Interesting results have been presented by Sammartano et al. [17] who tested several technologies for georeferencing of a castle and its vicinity. Accuracies achieved using the SLAM scanner GeoSLAM REVO were in centimeters, which corresponds well to our results.

Keitaaniemi et al. [37] discussed and tested the use of a combination of SLAM and a static terrestrial scanner for georeferencing indoor spaces. The accuracies detected in their study were also 0.05 m and better; they, however, evaluated accuracy only using several spherical targets in individual rooms of the mapped space so there were rather few points for a major statistical evaluation. Di Stefano et al. [18] scanned approximately 75 m long subterranean spaces, the walls of which were formed by chiseled stones and bricks. Three SLAM scanners were tested and compared to the results of a terrestrial scanner. They reported very good GeoSLAM Zeb Horizon accuracy (*RMSD* of 0.017 m). However, they used local transformation of a part of the cloud to the reference data (similar to if we had transformed each profile separately to the reference data), which artificially improved the results, and the global accuracy over the entire cloud was not reported.

The scanner from GeoSLAM for scanning bridge structures or other concrete structures is discussed, e.g., in Yuan et al. [38] and Ibrahimkhil et al. [39], but unfortunately, they only show the possibilities of use without testing the accuracy of the resulting cloud. Interesting accuracy testing can be found in Previtali et al. [40], where the beginning of the bridge structure is scanned using a Zeb Horizon scanner from GeoSLAM. The accuracy of the resulting data on the tested piece of structure is also consistent with the accuracy we report here for the original data without MLS or ICP. Unfortunately, the entire bridge was not scanned in the experiment and thus it is not possible to discuss the accuracy of the entire structure.

The accuracy characteristics achieved in our study are, considering the character of the object of the study and manufacturer-provided scanner parameters, very good. It should be noted that a bridge may not be an optimal object for SLAM scanning as it only covers a small part of the scanner view field. The original SLAM scanner data were characterized by a deviation from the reference cloud of approximately 0.02 m, which is a result sufficient for many applications, such as the creation of digital twins. Denoising SLAM scanner-acquired data using the MLS algorithm appears to be a useful approach, facilitating the processing and interpretation of data. When considering local accuracy after local (individual profiles) ICP transformation, i.e., evaluating the shape accuracy, the scanner yielded *RMSDs* as low as <0.01 m.

In terms of cost-effectiveness, the acquisition costs of SLAM scanners are nowadays comparable to those of terrestrial scanners. A SLAM scanner yields somewhat poorer accuracy (which may, however, be sufficient for many applications). On the other hand, the speed of data acquisition is a significant bonus, as the entire bridge structure was surveyed in about 30 min using the SLAM scanner compared to about 3 h when using the static terrestrial scanner.

5. Conclusions

In this paper, we evaluated the accuracy of the GeoSLAM Zeb Horizon SLAM scanner for the creation of a digital model of a bridge construction. Comparing the data with reference data from a high-accuracy terrestrial scanner and a total station, we yielded very good accuracies of the SLAM cloud across the entire bridge. Although SLAM data were significantly more noisy than data acquired using the static scanner, smoothing using the MLS method significantly improved the noise (although certain details, such as sharp

edges, were not preserved). For a 130 m long bridge, a global accuracy of 5 cm or better and local accuracies (evaluated using local ICP transformation of MLS-processed cloud as good as 5 mm) were achieved. Considering the speed and ease of scanning as well as the length of the bridge, the GeoSLAM Zeb Horizon results were very good, and using this scanner could be preferable to static scanners for applications such as creating digital twins, BIM, and their further use.

It should be strongly pointed out that this technology is definitely not suitable for improving the construction process nor supporting the construction/structural rectification of the bridge. For this purpose, it is necessary to use a precise total station, enabling the measurement of specific points with high accuracy.

Considering that a new generation of SLAM handheld scanners such as Emesent Hoovermap ST-X or Faro Orbis are already available, which have a significantly better measuring head (distance precision measurement enhanced to 1 cm (standard deviation) and number of channels to 32) and a new processing software, which can bring significantly better overall accuracy and lower noise in the data and therefore better capture of details, future research following this study could focus on comparing the previous and new generation of SLAM scanners and their measurement results.

Author Contributions: Conceptualization, R.U. and M.Š.; methodology, R.U.; software, M.Š.; validation, Ľ.K., P.B., and J.B.; formal analysis, T.S.; investigation, J.B.; resources, T.S.; data curation, J.B.; writing—original draft preparation, R.U.; writing—review and editing, M.Š.; visualization, M.Š.; supervision, Ľ.K.; project administration, R.U.; funding acquisition, R.U. All authors have read and agreed to the published version of the manuscript.

Institutional Review Board Statement: Not applicable.

Informed Consent Statement: Not applicable.

Data Availability Statement: The data presented in this study are available on request from the corresponding author. The data are not publicly available due to size of the data.

Conflicts of Interest: The authors declare no conflicts of interest.

References

1. Štroner, M.; Křemen, T.; Urban, R. Progressive Dilution of Point Clouds Considering the Local Relief for Creation and Storage of Digital Twins of Cultural Heritage. *Appl. Sci.* **2022**, *12*, 11540. [CrossRef]
2. Ding, Z.; Liu, S.; Liao, L.; Zhang, L. A Digital Construction Framework Integrating Building Information Modeling and Reverse Engineering Technologies for Renovation Projects. *Autom. Constr.* **2019**, *102*, 45–58. [CrossRef]
3. Wagg, D.J.; Worden, K.; Barthorpe, R.J.; Gardner, P. Digital Twins: State-of-the-Art and Future Directions for Modeling and Simulation in Engineering Dynamics Applications. *ASCE ASME J. Risk Uncertain. Eng. Syst. Part B Mech. Eng.* **2020**, *6*, 030901. [CrossRef]
4. Erdélyi, J.; Honti, R.; Funtík, T.; Mayer, P.; Madiev, A. Verification of Building Structures Using Point Clouds and Building Information Models. *Buildings* **2022**, *12*, 2218. [CrossRef]
5. Hosamo, H.H.; Hosamo, M.H. Digital Twin Technology for Bridge Maintenance Using 3D Laser Scanning: A Review. *Adv. Civ. Eng.* **2022**, *2022*, 2194949. [CrossRef]
6. Armesto, J.; Lubowiecka, I.; Ordóñez, C.; Rial, F.I. FEM Modeling of Structures Based on Close Range Digital Photogrammetry. *Autom. Constr.* **2009**, *18*, 559–569. [CrossRef]
7. Koska, B.; Křemen, T. The Combination of Laser Scanning and Structure from Motion Technology for Creation of Accurate Exterior and Interior Orthophotos of St. Nicholas Baroque Church. *Int. Arch. Photogramm. Remote Sens. Spat. Inf. Sci.* **2013**, *XL-5/W1*, 133–138. [CrossRef]
8. Pukanská, K.; Bartoš, K.; Bella, P.; Gašinec, J.; Blistan, P.; Kovanič, Ľ. Surveying and High-Resolution Topography of the Ochtiná Aragonite Cave Based on TLS and Digital Photogrammetry. *Appl. Sci.* **2020**, *10*, 4633. [CrossRef]
9. Moudrý, V.; Cord, A.F.; Gábor, L.; Laurin, G.V.; Barták, V.; Gdulová, K.; Malavasi, M.; Rocchini, D.; Stereńczak, K.; Prošek, J.; et al. Vegetation Structure Derived from Airborne Laser Scanning to Assess Species Distribution and Habitat Suitability: The Way Forward. *Divers. Distrib.* **2022**, *29*, 39–50. [CrossRef]

10. Rybansky, M. Determination of Forest Structure from Remote Sensing Data for Modeling the Navigation of Rescue Vehicles. *Appl. Sci.* **2022**, *12*, 3939. [CrossRef]

11. Jon, J.; Koska, B.; Pospíšil, J. Autonomous Airship Equipped by Multi-Sensor Mapping Platform. *Int. Arch. Photogramm. Remote Sens. Spat. Inf. Sci.* **2013**, *XL-5/W1*, 119–124. [CrossRef]

12. Ayele, Y.Z.; Aliyari, M.; Griffiths, D.; Droguett, E.L. Automatic Crack Segmentation for UAV-Assisted Bridge Inspection. *Energies* **2020**, *13*, 6250. [CrossRef]

13. Forcael, E.; Román, O.; Stuardo, H.; Herrera, R.F.; Soto-Muñoz, J. Evaluation of Fissures and Cracks in Bridges by Applying Digital Image Capture Techniques Using an Unmanned Aerial Vehicle. *Drones* **2024**, *8*, 8. [CrossRef]

14. Mandirola, M.; Casarotti, C.; Peloso, S.; Lanese, I.; Brunesi, E.; Senaldi, I. Use of UAS for Damage Inspection and Assessment of Bridge Infrastructures. *Int. J. Disaster Risk Reduct.* **2022**, *72*, 102824. [CrossRef]

15. Kopáčik, A.; Kajánek, P.; Brindza, J.; Erdélyi, J.; Kyrinovič, P. Development of A Mobile Mapping System for Simultaneous Localization and Mapping. In Proceedings of the 22nd International Multidisciplinary Scientific GeoConference SGEM 2022, STEF92 Technology, Albena, Bulgaria, 4–10 July 2022. [CrossRef]

16. Kalvoda, P.; Nosek, J.; Kuruc, M.; Volařík, T.; Kalvodova, P. Accuracy Evaluation and Comparison of Mobile Laser Scanning and Mobile Photogrammetry Data. In Proceedings of the 6th World Multidisciplinary Earth Sciences Symposium, Prague, Czech Republic, 7–11 September 2020; IOP Conference Series: Earth and Environmental Science. IOP Publishing Ltd.: Bristol, UK, 2020; pp. 1–10. [CrossRef]

17. Sammartano, G.; Spanò, A. Point Clouds by SLAM-Based Mobile Mapping Systems: Accuracy and Geometric Content Validation in Multisensor Survey and Stand-Alone Acquisition. *Appl. Geomat.* **2018**, *10*, 317–339. [CrossRef]

18. Di Stefano, F.; Torresani, A.; Farella, E.M.; Pierdicca, R.; Menna, F.; Remondino, F. 3D Surveying of Underground Built Heritage: Opportunities and Challenges of Mobile Technologies. *Sustainability* **2021**, *13*, 13289. [CrossRef]

19. Cramer, M.; Przybilla, H.-J.; Zurhorst, A. UAV Cameras: Overview and Geometric Calibration Benchmark. *Int. Arch. Photogramm. Remote Sens. Spat. Inf. Sci.* **2017**, *XLII-2/W6*, 85–92. [CrossRef]

20. Przybilla, H.-J.; Bäumker, M.; Luhmann, T.; Hastedt, H.; Eilers, M. Interaction between Direct Georeferencing, Control Point Configuration and Camera Self-Calibration for RTK-Based UAV Photogrammetry. *Int. Arch. Photogramm. Remote Sens. Spat. Inf. Sci.* **2020**, *XLIII-B1-2020*, 485–492. [CrossRef]

21. Teppati Losè, L.; Chiabrando, F.; Giulio Tonolo, F. Boosting the Timeliness of UAV Large Scale Mapping. Direct Georeferencing Approaches: Operational Strategies and Best Practices. *ISPRS Int. J. Geo-Inf.* **2020**, *9*, 578. [CrossRef]

22. Kingsland, K. Comparative Analysis of Digital Photogrammetry Software for Cultural Heritage. *Digit. Appl. Archaeol. Cult. Herit.* **2020**, *18*, e00157. [CrossRef]

23. Štroner, M.; Urban, R.; Seidl, J.; Reindl, T.; Brouček, J. Photogrammetry Using UAV-Mounted GNSS RTK: Georeferencing Strategies without GCPs. *Remote Sens.* **2021**, *13*, 1336. [CrossRef]

24. Adhikari, M.D.; Kim, T.-H.; Yum, S.-G.; Kim, J.-Y. Damage Detection and Monitoring of a Concrete Structure using 3D Laser Scanning. *Eng. Proc.* **2023**, *36*, 1. [CrossRef]

25. Fareed, N.; Flores, J.P.; Das, A.K. Analysis of UAS-LiDAR Ground Points Classification in Agricultural Fields using Traditional Algorithms and PointCNN. *Remote Sens.* **2023**, *15*, 483. [CrossRef]

26. Xu, Z.; Liang, Y.; Lu, H.; Kong, W.; Wu, G. An Approach for Monitoring Prefabricated Building Construction Based on Feature Extraction and Point Cloud Segmentation. *Eng. Constr. Archit. Manag.* **2022**, *30*, 5302–5332. [CrossRef]

27. Jiang, R.; Jáuregui, D.V.; White, K.R. Close-Range Photogrammetry Applications in Bridge Measurement: Literature Review. *Measurement* **2008**, *41*, 823–834. [CrossRef]

28. Graves, W.; Aminfar, K.; Lattanzi, D. Full-Scale Highway Bridge Deformation Tracking via Photogrammetry and Remote Sensing. *Remote Sens.* **2022**, *14*, 2767. [CrossRef]

29. Mohammadi, M.; Rashidi, M.; Mousavi, V.; Karami, A.; Yu, Y.; Samali, B. Quality Evaluation of Digital Twins Generated Based on UAV Photogrammetry and TLS: Bridge Case Study. *Remote Sens.* **2021**, *13*, 3499. [CrossRef]

30. Chen, W.; Zhou, C.; Shang, G.; Wang, X.; Li, Z.; Xu, C.; Hu, K. SLAM Overview: From Single Sensor to Heterogeneous Fusion. *Remote Sens.* **2022**, *14*, 6033. [CrossRef]

31. Akpınar, B. Performance of Different SLAM Algorithms for Indoor and Outdoor Mapping Applications. *Appl. Syst. Innov.* **2021**, *4*, 101. [CrossRef]

32. Taheri, H.; Xia, Z.C. SLAM; Definition and Evolution. *Eng. Appl. Artif. Intell.* **2021**, *97*, 104032. [CrossRef]

33. Štroner, M.; Urban, R.; Línková, L. A New Method for UAV Lidar Precision Testing Used for the Evaluation of an Affordable DJI ZENMUSE L1 Scanner. *Remote Sens.* **2021**, *13*, 4811. [CrossRef]

34. Alexa, M.; Behr, J.; Cohen-Or, D.; Fleishman, S.; Levin, D.; Silva, C.T. Computing and Rendering Point Set Surfaces. *IEEE Trans. Vis. Comput. Graph.* **2003**, *9*, 3–15. [CrossRef]

35. Tiozzo Fasiolo, D.; Scalera, L.; Maset, E. Comparing LiDAR and IMU-Based SLAM Approaches for 3D Robotic Mapping. *Robotica* **2023**, *41*, 2588–2604. [CrossRef]

36. Wajs, J.; Kasza, D.; Zagożdżon, P.P.; Zagożdżon, K.D. 3D Modeling of Underground Objects with the Use of SLAM Technology on the Example of Historical Mine in Ciechanowice (Ołowiane Range, The Sudetes). *E3S Web Conf.* **2018**, *29*, 00024. [CrossRef]

37. Keitaanniemi, A.; Virtanen, J.-P.; Rönnholm, P.; Kukko, A.; Rantanen, T.; Vaaja, M.T. The Combined Use of SLAM Laser Scanning and TLS for the 3D Indoor Mapping. *Buildings* **2021**, *11*, 386. [CrossRef]

38. Yuan, X.; Smith, A.; Moreu, F.; Sarlo, R.; Lippitt, C.D.; Hojati, M.; Alampalli, S.; Zhang, S. Automatic Evaluation of Rebar Spacing and Quality Using LiDAR Data: Field Application for Bridge Structural Assessment. *Autom. Constr.* **2023**, *146*, 104708. [CrossRef]
39. Ibrahimkhil, M.H.; Shen, X.; Barati, K.; Wang, C.C. Dynamic Progress Monitoring of Masonry Construction through Mobile SLAM Mapping and As-Built Modeling. *Buildings* **2023**, *13*, 930. [CrossRef]
40. Previtali, M.; Brumana, R.; Banfi, F. Existing Infrastructure Cost Effective Informative Modelling with Multisource Sensed Data: TLS, MMS and Photogrammetry. *Appl. Geomat.* **2020**, *14*, 21–40. [CrossRef]